Enhanced thermoelectric performance of optimized Yb-filled and Fe-substituted skutterudite compounds Yb0.6FexCo4−xSb12

Enhanced thermoelectric performance of optimized Yb-filled and Fe-substituted skutterudite compounds $Yb_{0.6}Fe_xCo_{4-x}Sb_{12}$

Yuqi Chen[*], Yukihiro Kawamura, Junichi Hayashi, and Chihiro Sekine[†]

Muroran Institute of Technology, Muroran, Hokkaido 050-8585, Japan

Optimized Yb-filled Fe-substituted skutterudites $Yb_{0.6}Fe_xCo_{4-x}Sb_{12}$ (x=0, 0.5, and 1.0) were synthesized using a high-pressure technique. The samples were characterized by powder X-ray diffraction (XRD) analysis and electron probe microanalysis (EPMA). The thermoelectric transport properties of the samples such as Seebeck coefficient, electrical conductivity, carrier concentration, and thermal conductivity were studied in the temperature range of 2-300 K. With 1/8 Fe substitution for the Co site (x=0.5), the Seebeck coefficient and thermal conductivity were obviously optimized. Carrier concentration analysis indicates that proper Fe substitution can effectively compensate for the excess electrons and optimize the electric transport properties. The reduction in the total thermal conductivity κ could be mainly caused by the reduction in electron contribution to κ. Compared with an only-Yb-filled compound, a 26% improved figure of merit ZT was achieved at 300 K at the Fe substitution ratio x=0.5 (ZT= 0.11). This result confirms that Fe substitution on the Co site is an effective approach to tuning and optimizing the thermoelectric properties of $CoSb_3$-based skutterudites.

1. Introduction

Thermoelectric (TE) materials, which can directly convert heat into electricity or vice visa, play an important role in providing globally sustainable energy.[1] The intrinsic performance of thermoelectric materials is estimated on the basis of the dimensionless figure of merit ZT, defined as $ZT = S^2 T / \rho \cdot \kappa$, where S, ρ, and κ are the Seebeck coefficient, electrical resistivity, and total thermal conductivity, respectively. To achieve a high ZT, an ideal TE material should have two desirable features: it can prevent phonon propagation like glass but can conduct electrons like crystals (PGEC).[2]

Skutterudite compounds with an open structure [cubic unit cell ($Im\bar{3}$) with two fillable interstitial voids at the 2a positions (12-coordinated)] have been actively studied as canonical PGEC materials owing to their excellent thermoelectric properties and flexibly tunable electric and lattice properties.[3–5] Among members of the skutteru-

---

dite family, $CoSb_3$ shows excellent thermoelectric properties. However, its high thermal conductivity restricts its applications.[6] It has been well proved that filling the Sb-icosahedron voids in $CoSb_3$ with heavy Yb atoms can notably decrease the thermal conductivity.[7–13] Previous research findings suggest that the appropriate Yb doping ratio should be approximately 0.2 because a higher Yb doping ratio increases the electric carrier concentration, which would lead to a reduction in Seebeck coefficient and thus a low figure of merit.[14,15] On the other hand, a higher Yb doping ratio contributes to the decrease in thermal conductivity. Therefore, a higher figure of merit should be achievable if the excess electrons generated owing to highly doped Yb can be properly compensated.

Fe is considered a hole doping element for Co-site substitution because it has one less 3d electron than Co while keeping a similar atomic radius to Co.[16–18] Various studies about the thermoelectric properties of Yb-filled or/and Fe-substituted $CoSb_3$ skutterudite compounds have been carried out.[9,19–26] However, in most of them, the Fe substitution ratio was fixed and the effects of different rare-earth fillers on the TE properties were focused on. For example, the crystal structure and TE properties of $Yb_xCo_{2.5}Fe_{1.5}Sb_{12}$ have been reported by Dong $et\ al.$[20] Kim $et\ al.$ synthesized various $Ti_xCo_3Fe_1Sb_{12}$ ($0 \leq x \leq 0.8$) compounds and studied the effects of Ti filling ratio on the TE properties.[25] Park $et\ al.$ studied the effects of Fe substitution ratio on the TE performance of $Co_{1-x}Fe_xSb_3$ compounds.[26] There is barely any information about Yb-ratio-fixed and Fe-ratio-varied compounds, which are necessary for studying the effects of Fe substitution on the TE properties of Yb-filled skutterudites.

We previously reported the highest actual Yb doping ratio of 0.29 in the compound with the nominal composition $Yb_{0.6}Co_4Sb_{12}$ (actual composition, $Yb_{0.29}Co_4Sb_{12}$) prepared using a high-pressure synthesis technique.[27] The lattice thermal conductivity of $Yb_{0.6}Co_4Sb_{12}$ is minimum at 300 K, but the Seebeck coefficient of the compound is decreased owing to its high electron concentration. To further optimize the figure of merit, the excess electrons in $Yb_{0.6}Co_4Sb_{12}$ need to be compensated. Therefore, we studied the optimized Yb-filled Fe-substituted compounds $Yb_{0.6}Fe_xCo_{4-x}Sb_{12}$ (x=0, 0.5, and 1.0) in detail. We hope that this work will provide a link to previous works and allow for a direct comparison of the effects of Fe doping ratio on the thermoelectric properties of Yb-filled $CoSb_3$ skutterudites.

2. Experimental methods

Fe-substituted $Yb_{0.6}Fe_xCo_{4-x}Sb_{12}$ compounds with x=0, 0.5, and 1.0 were synthesized using a cubic-anvil high-pressure apparatus. Unfilled $CoSb_3$ was also synthesized under the same conditions as a reference. The samples were prepared by reacting stoichiometric amounts of 3N (99.9% pure)-Yb, 3N-Fe, 4N-Co and 6N-Sb powders at 2 GPa and kept at 590 °C for 120 min. The details about the preparation are described in our previous papers.[28,29]

A synthesized sample was a cylindrical shape with 3 mm in diameter and 7 mm in height. The crystalline phases of the synthesized samples were characterized by XRD analysis using Co $K_{\alpha 1}$ radiation and silicon as a standard. The lattice parameters of the samples were calculated by the least-squares fitting method. To determine the actual element distribution and Yb doping content, the face and point analysis (beam size 50 μm) of EPMA (JEOL JXA-8900R) of all compounds were performed. For the point analysis, five or six different points were carefully chosen to reduce errors.

Electrical conductivity was measured by a standard DC four-probe method. The Seebeck coefficient and thermal conductivity were measured by physical property measuring system (PPMS; Quantum Design) with a thermal transport option. The Hall effect was measured by the van der Pauw method using a constant magnetic field of 0.1 T. The carrier concentration n was calculated from the Hall coefficient R_H with the relationship $n = 1/|R_H|e$, where e is the elementary electron charge. All transport data have been carried out at 2-300 K.

3. Results and discussion

Figure 1 shows the powder X-ray diffraction patterns of $CoSb_3$ and $Yb_{0.6}Fe_xCo_{4-x}Sb_{12}$ (x=0, 0.5, 1.0) samples. High-purity Fe-substituted $Yb_{0.6}Fe_xCo_{4-x}Sb_{12}$ compounds were prepared at 590 °C for 120 min at 2 GPa. The observed diffraction lines were indexable using the skutterudite structure with a trace of second phases ($\leq$ 4%). The lattice parameters were calculated to examine the comprehensive effects of Yb doping and Fe substitution, as shown in the inset of Fig. 1. It was observed that Yb doping led to a sharp increase in lattice constant, revealing a large expansion of the unit cell. The Fe substitution, however, does not show an obvious effect on lattice constant. This result is contradictory to those of previous works.[7,22,30,31] The reason for the lattice constant discrepancy might be attributed to the high filling ratio of Yb and the relatively low ratio of Fe substitution (that is, only 1/8 or 2/8 Co site was substituted by Fe). Similar
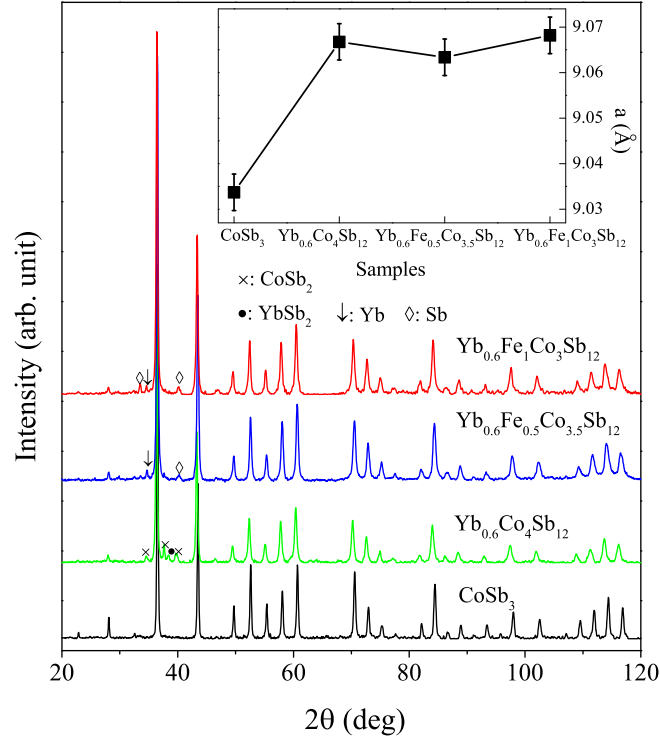
Fig. 1. (Color online) X-ray diffraction patterns of $CoSb_3$ and $Yb_{0.6}Fe_xCo_{4-x}Sb_{12}$ (x=0, 0.5, and 1.0) prepared at 2 GPa. The second phases of $CoSb_2$, $YbSb_2$, Yb, and Sb were indicated by $\times$, $\bullet$, $\downarrow$, and $\Diamond$, respectively.
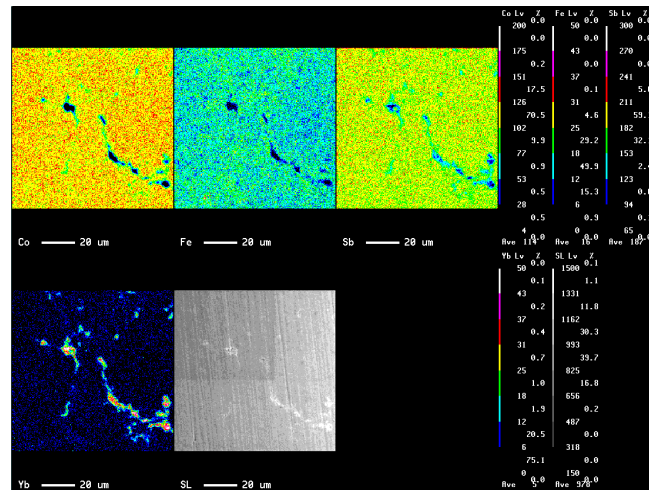
Fig. 2. (Color online) Element distribution mapping of $Yb_{0.6}Fe_{0.5}Co_{3.5}Sb_{12}$ by EPMA.

behaviors were also observed in $Mm_yFe_xCo_{4-x}Sb_{12}$ skutterudites synthesized by the hot pressing method.[24] From the stable unit cell volume of $Yb_{0.6}Fe_xCo_{4-x}Sb_{12}$ compounds, we can deduce that the rattling vibration of Yb fillers in all compounds should be similar.

Table I. Summary of compositions and secondary phases.

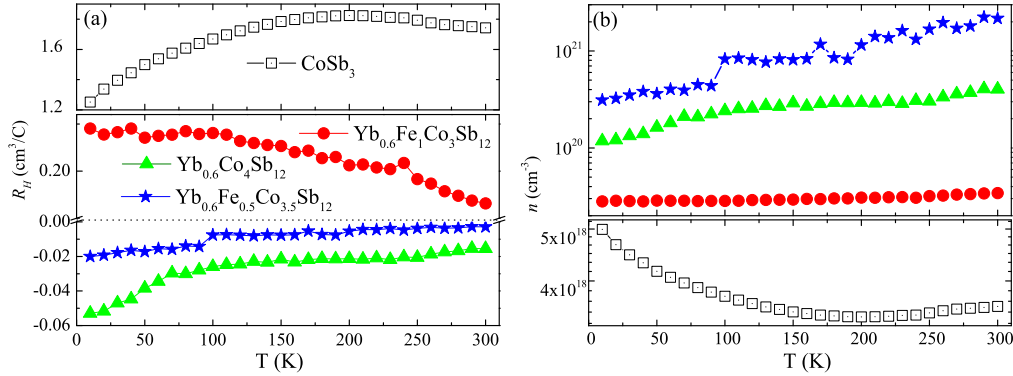| Nominal composition	Actual composition	Secondary phases ($\leq 4\%$)
Co_4Sb_{12}	$Co_4Sb_{11.7}$	None
$Yb_{0.6}Co_4Sb_{12}$	$Yb_{0.29}Co_4Sb_{12}$	Yb; $(Yb, Co)Sb_2$
$Yb_{0.6}Fe_{0.5}Co_{3.5}Sb_{12}$	$Yb_{0.47}Fe_{0.38}Co_{3.62}Sb_{12.4}$	Yb; Sb; $FeSb_2$
$Yb_{0.6}Fe_1Co_3Sb_{12}$	$Yb_{0.29}Fe_{0.76}Co_{3.24}Sb_{12.5}$	Yb; Sb; $(Fe, Co)Sb_2$; Yb_2Sb_5

Fig. 3. (Color online) Temperature dependence of (a) Hall coefficient R_H and (b) carrier concentration n for $Yb_{0.6}Fe_xCo_{4-x}Sb_{12}$.

Figure 2 shows the element distribution mapping of $Yb_{0.6}Fe_{0.5}Co_{3.5}Sb_{12}$ by EPMA. As shown in Fig. 2, all the elements are homogeneously distributed in the skutterudite matrix. Some local Fe-rich segments (indicative of Yb and $FeSb_2$) are also observed in $Yb_{0.6}Fe_{0.5}Co_{3.5}Sb_{12}$.

Table I shows the actual composition and secondary phases determined by the point analysis of EPMA and XRD results. As the parent compound, $CoSb_3$ is also included for comparison. By substituting small quantities of Fe on the Co site, the actual filling fraction of Yb was markedly increased. These results indicate that Yb atoms can easily enter into the voids when some of the Co sites were replaced by Fe. As the filling fraction of Yb is relevant with the electronegativity of Sb, it might be speculated that the replacement of Fe on the Co site affected the charge distribution of adjacent Sb atoms.

Figure 3 shows the temperature dependence of the Hall coefficient R_H [Fig. 3(a)] and the carrier concentration n [Fig. 3(b)] in $Yb_{0.6}Fe_xCo_{4-x}Sb_{12}$. The Hall coefficient and carrier concentration of $CoSb_3$ are shown for comparison. Unfilled $CoSb_3$ shows typically p-type semiconductor behaviors, whereas Yb-doped Fe-substituted compounds behave

similarly to semimetallic compounds. It is found that the Hall coefficient is negative for x = 0 and 0.5, and positive for x = 1.0. Compared with the only Yb doping compound ($Yb_{0.6}Co_4Sb_{12}$), the absolute value of the Hall coefficient of $Yb_{0.6}Fe_{0.5}Co_{3.5}Sb_{12}$ was markedly decreased with a low ratio of Fe substitution for Co, reflecting that Fe successfully worked as a hole donor. As for a higher ratio of Fe substitution (x=1.0), the sign of the Hall coefficient shifted from negative to positive, indicating that the main carriers changed from electrons to holes. As shown in Fig. 3(b), the carrier concentration first increases with 1/8 Fe substitution for Co sites and then decreases for 2/8 Fe substitution. Theoretically, the carrier concentration should continuously decrease with increasing Fe substitution ratio because each Fe atom provides one hole into a unit cell and the filler loses electrons to compensate for the holes. However, the carrier concentration of $Yb_{0.6}Fe_{0.5}Co_{3.5}Sb_{12}$ is higher than that of $Yb_{0.6}Co_4Sb_{12}$. This anomalous behavior should be attributed to the increased Yb filling fraction accompanying Fe substitution (Table I).
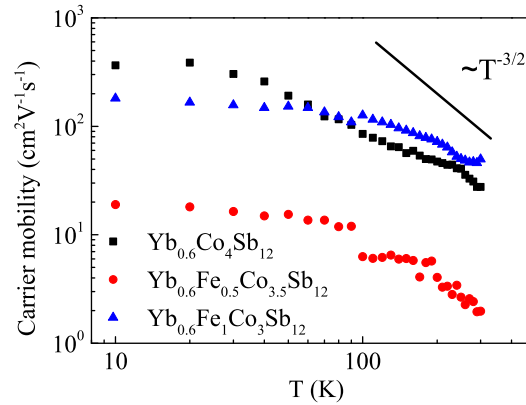
Fig. 4.   (Color online) Temperature dependence of carrier mobility for $Yb_{0.6}Fe_xCo_{4-x}Sb_{12}$.

Combining the Hall effect data with the behavior of electrical resistivity, carrier mobility can be obtained. Figure 4 shows the temperature dependence of carrier mobility. The carrier mobility follows well the $T^{-3/2}$ behavior above 150 K, which indicates that the primary carrier scattering process is acoustic phonon scattering, which controls high-temperature thermal transport properties. As temperature decreases, the temperature dependence of carrier mobility gradually deviates from the $T^{-3/2}$ behavior and saturates below 20 K, suggesting that the predominant source of scattering gradually changes from phonons to neutral impurities. The anomalous behavior of $Yb_{0.6}Fe_1Co_3Sb_{12}$ at

high temperatures might arise from the segregation of impurity phases (Yb, Sb, FeSb$_2$, CoSb$_2$, and Yb$_2$Sb$_5$), as also indicated both by XRD analysis and EPMA.
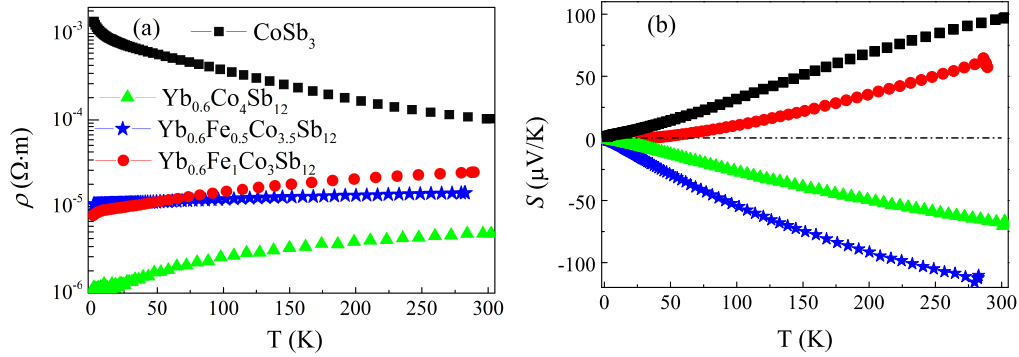
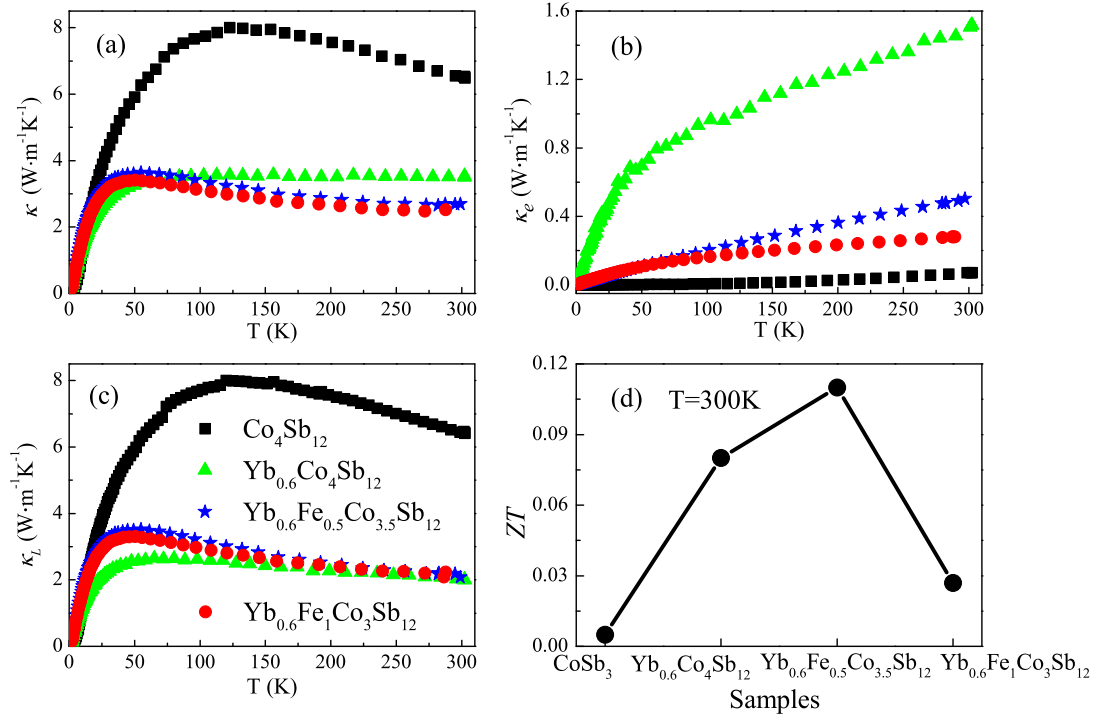**Fig. 5.** (Color online) Temperature dependance of (a) the electrical resistivity ρ and (b) the Seebeck coefficient S for Yb$_{0.6}$Fe$_x$Co$_{4-x}$Sb$_{12}$.

Figures 5(a) and 5(b) show the electrical resistivity ρ and the Seebeck coefficient S of all specimens over the temperature range of 2-300 K, respectively. As shown in Fig. 5(a), Yb filling leads to a marked reduction in ρ in compound Yb$_{0.6}$Co$_4$Sb$_{12}$. However, Fe substitution deteriorates ρ by a factor of almost one-half (Yb$_{0.6}$Fe$_{0.5}$Co$_{3.5}$Sb$_{12}$ and Yb$_{0.6}$Fe$_1$Co$_3$Sb$_{12}$). The ρ values of both Yb$_{0.6}$Co$_4$Sb$_{12}$ and Yb$_{0.6}$Fe$_1$Co$_3$Sb$_{12}$ increase with increasing temperature. In addition, the ρ of Yb$_{0.6}$Fe$_{0.5}$Co$_{3.5}$Sb$_{12}$ behaves almost independently of temperature. This behavior has also been reported with the explanation that the Fe-substituted CoSb$_3$ is a degenerated semiconductor and its electrical resistivity is independent of temperature owing to the charge carrier scattering.[32,33]

Figure 5(b) shows the temperature dependence of the Seebeck coefficient over the temperature range of 2-300 K. Compared with the only-Yb-filled Yb$_{0.6}$Co$_4$Sb$_{12}$ compound, the 1/8 Fe substitution (x=0.5) in the Co site results in a 41% increase in S at 300 K. The maximum S at room temperature is -116 μV/K for Yb$_{0.6}$Fe$_{0.5}$Co$_{3.5}$Sb$_{12}$ (4.03×10^{20} cm^{-3}), which is even comparable to the double rare-earth-filled skutterudites Ba$_{0.24}$Yb$_{0.19}$Fe$_{0.38}$Co$_{3.63}$Sb$_{12}$.[21] Higher Fe substitution ratio (x=1.0) does not show further increase in the absolute value of S but leads to conversion from negative to positive. The sign conversation of S is in accordance with R_H and indicates that the major carriers in the compound change from electrons to holes as the Fe ratio increases. This result corroborates the observation that Fe has been successfully introduced as a hole dopant. Proper Fe substitution can improve the thermoelectric properties.

Figure 6(a) shows plots of the thermal conductivity κ in Yb$_{0.6}$Fe$_x$Co$_{4-x}$Sb$_{12}$. It can

Fig. 6. (Color online) Temperature dependences of (a) thermal conductivity κ, (b) electronic thermal conductivity κ_e, (c) lattice thermal conductivity κ_L, and (d) ZT values from 0 to 300 K for $Yb_{0.6}Fe_xCo_{4-x}Sb_{12}$.

be observed that the thermal conductivity is apparently diminished not only by Yb filling but also by Fe substitution on the Co site. The lowest κ of 2.5 W m^{-1} K^{-1} is obtained in $Yb_{0.6}FeCo_3Sb_{12}$ at room temperature.

The electronic thermal conductivity component κ_e was calculated from the Wiedemann-Franz law as $\kappa_e = L_0T/\rho$, where L_0 denotes the Lorenz number and has a numerical value of $L_0 = 2.44 \times 10^{-8}$ V^2/K^2, T is the absolute temperature, and ρ is the electrical resistivity. The lattice thermal conductivity κ_L can be obtained by subtracting the electronic thermal conductivity κ_e from the total thermal conductivity κ. The temperature dependences of κ_e and κ_L in $Yb_{0.6}Fe_xCo_{4-x}Sb_{12}$ are shown in Figs. 6(b) and 6(c), respectively. In principle, one should consider the effects of Fe substitution on κ in the entire temperature range. However, we focused on the effects of Fe substitution on phonon scattering near room temperature since the dominant scattering mechanism is impurity scattering in the low-temperature range.

As shown in Fig. 6(b), the room temperature κ_e was markedly decreased by Fe substitution (1.5 W m^{-1} K^{-1} in $Yb_{0.6}Co_4Sb_{12}$ but only 0.3 W m^{-1} K^{-1} in $Yb_{0.6}Fe_1Co_3Sb_{12}$). If the decrease in κ_e originates from the fluctuation of Yb content, the κ_e values of

$Yb_{0.6}Co_4Sb_{12}$ ($Yb_{0.29}Co_4Sb_{12}$) and $Yb_{0.6}Fe_1Co_3Sb_{12}$ ($Yb_{0.29}Fe_{0.76}Co_{3.24}Sb_{12.5}$) should be similar because of the similar Yb contents. However, $Yb_{0.6}Fe_1Co_3Sb_{12}$ shows an apparent reduction in κ_e compared with $Yb_{0.6}Co_4Sb_{12}$. Therefore, the large decrease in κ_e might be related to the actual Fe:Co ratio.[31] Different from the behavior of κ_e, although the actual Yb-Fe fraction fluctuates, the room temperature κ_L is almost not affected by Fe substitution [Fig. 6(c)]. On the basis of the results on the lattice constant, it might be deduced that Fe substitution does not introduce additional phonon scattering. This may be a reason why κ_L at around room temperature remains unchanged. Combining Figs. 6(b) and 6(c), it appears that the decrease in κ at room temperature mainly originates from the decrease in κ_e.

Figure 6(d) shows the dimensionless figure of merit ZT of all compounds at 300 K. Compared with that of $Yb_{0.6}Co_4Sb_{12}$, the ZT of $Yb_{0.6}Fe_{0.5}Co_{3.5}Sb_{12}$ is clearly improved. The highest ZT (0.11) was achieved in $Yb_{0.6}Fe_{0.5}Co_{3.5}Sb_{12}$ at 300 K. This value is even higher than those of double Ba- and Yb-filled Fe-substituted compounds ($ZT=$ 0.05 at 300 K and $ZT=$ 0.6 at 800 K).[34] Moreover, the ZT of $Yb_{0.6}Fe_{0.5}Co_{3.5}Sb_{12}$ at 300 K is comparable to that of a similar compound ($Yb_xFe_yCo_{4-y}Sb_{12}$) reported by Dong *et al.*,[9,20] in which $ZT=$ 0.8 at around 800 K. Therefore, a higher ZT in $Yb_{0.6}Fe_{0.5}Co_{3.5}Sb_{12}$ can be achieved in the high-temperature range.

4. Conclusions

High-quality $Yb_{0.6}Fe_xCo_{4-x}Sb_{12}$ ($x \leq 1.0$) samples were synthesized by a high-pressure and high-temperature method. The Fe-substitution effects on the TE transport properties of $Yb_{0.6}Co_4Sb_{12}$ were studied from the viewpoints of both electrical and thermal transport properties. The Seebeck coefficient S was increased but the electric resistivity ρ also was increased by the 1/8 Fe substitution of the Co site. The variations of S and ρ originate from the change in carrier concentration. The optimized thermal conductivity κ in $Yb_{0.6}Fe_{0.5}Co_{3.5}Sb_{12}$ is mainly attributed to the decrease in the electron conductivity κ_e. As a consequence, the optimized figure of merit ZT of 0.11 at 300 K was achieved in $Yb_{0.6}Fe_{0.5}Co_{3.5}Sb_{12}$, which is 26% higher than that in the only-Yb-filled skutterudite $Yb_{0.6}Co_4Sb_{12}$.

References

1) G. J. Snyder and E. S. Toberer, Nat. Mater. **7**, 105 (2008).

2) G. A. Slack, in *CRC Handbook of Thermoelectrics.* ed. D. M. Rowe (CRC Press, Boca Raton, FL, 1995) chap. 34.

3) B. C. Sales, D. Mandrus, B. C. Chakoumakos, V. Keppens, and J. R. Thompson, Phys. Rev. B **56**, 15081 (1997).

4) C. Uher, J. Yang, and S. Hu, MRS Proc. **545**, 247 (1998).

5) U. Ctirad, in *Thermoelectrics handbook*, ed. D . M . Rowe (CRC Press, Boca Raton, FL, 2005) Chap. 34.

6) T. Caillat, A. Borshchevsky, and J. P. Fleurial, J. Appl. Phys. **80**, 4442 (1996).

7) A. Borshchevsky, T. Caillat, and J. P. Fleurial, 15th Int. Conf. IEEE Thermoelectrics, 1996, p. 112.

8) G. S. Nolas, G. A. Slack, D. T. Morelli, T. M. Tritt, and A. C. Ehrlich, J. Appl. Phys. **79**, 4002 (1996).

9) Y. Dong, P. Puneet, T. M. Tritt, and G. S. Nolas, Phys. Status Solidi: Rapid Res. Lett. **7**, 418 (2013).

10) I. K. Dimitrov, M. E. Manley, S. M. Shapiro, J. Yang, W. Zhang, L. Chen, Q. Jie, G. Ehlers, A. Podlesnyak, and J. Camacho, Phys. Rev. B **82**, 174301 (2010).

11) X. Y. Zhao, X. Shi, L. D. Chen, W. Q. Zhang, S. Q. Bai, Y. Z. Pei, X. Y. Li, and T. Goto, Appl. Phys. Lett. **89**, 092121 (2006).

12) G. S. Nolas, J. Cohn, and G. A. Slack, Phys. Rev. B **58**, 164 (1998).

13) J. Nagao, D. Nataraj, M. Ferhat, T. Uchida, S. Takeya, T. Ebinuma, H. Anno, K. Matsubara, E. Hatta, and K. Mukasa, J. Appl. Phys. **92**, 4135 (2002).

14) G. S. Nolas, M. Kaeser, and T. M. Tritt, Appl. Phys. Lett. **77**, 1855 (2000).

15) K. T. Wojciechowski, Mater. Ceram. **62**, 461 (2010).

16) E. Matsuoka, K. Tanaka, S. Morimoto, T. Sasakawa, and T. Takabatake, Jpn. J. Appl. Phys. **45**, 4025 (2006).

17) E. Bauer, A. Galatanu, H. Michor, G. Hilscher, P. Rogl, P. Boulet, and H. Noël, Eur. Phys. J. B **14**, 483 (2000).

18) L. Chen, X. Tang, T. Goto, and T. Hirai, J. Mater. Res. **15**, 2276 (2000).

19) K.-H. Park, S. Lee, W.-S. Seo, D.-K. Shin, and I.-H. Kim, J. Korean Phys. Soc. **64**, 863 (2014).

20) Y. Dong, P. Puneet, T. M. Tritt, and G.S. Nolas, J. Solid State Chem. **209**, 1

(2014).

21) S. Ballikaya, and C. Uher, J. Alloys Compd. **585**, 168 (2014).

22) C. Zhou, D. Morelli, X. Zhou, G. Wang, and C. Uher, Intermetallics **19**, 1390 (2011).

23) R. Liu, J. Yang, X. Chen, X. Shi, L. Chen, and C. Uher, Intermetallics **19**, 1747 (2011).

24) L. Zhang, A. Grytsiv, M. Kerber, P. Rogl, E. Bauer, and M. Zehetbauer, J. Alloys Compd. **490**, 19 (2010).

25) D. Kim, K. Kurosaki, Y. Ohishi, H. Muta and S. Yamanaka, APL Mater. **1**, 032115 (2013).

26) K. Park, J. Jung, S.-C. Ur, and H. Kim, Phy. Scr. **T139**, 014009 (2010).

27) Y. Chen, Y. Kawamura, J. Hayashi, and C. Sekine, Jpn. J. Appl. Phys. **54**, 055501 (2015).

28) I. Shirotani, K. Takeda, C. Sekine, J. Hayashi, R. Nakada, K. Kihou, Y. Ohishi, and T. Yagi, Z. Naturforsch. B **61**, 1471(2006).

29) C. Sekine, K. Akita, N. Yanase, I. Shirotani, I. Inagawa, and C.-H. Lee, Jpn. J. Appl. Phys. **40**, 3326 (2001).

30) D. Bérardan, C. Godart, E. Alleno, E. Leroy, and P. Rogl, J. Alloys Compd. **350**, 30 (2003).

31) J. Yang, G. P. Meisner, D. T. Morelli, and C. Uher, Phys. Rev. B **63**, 014410 (2000).

32) I.-H. Kim, and S.-C. Ur, Mater. Lett. **61**, 2446 (2007).

33) S. Katsuyama, Y. Shichijo, M. Ito, K. Majima, and H. Nagai, J. Appl. Phys. **84**, 6708 (1998).

34) Y. Dong, P. Puneet, T. M. Tritt, and G. S. Nolas, J. Mater. Sci. **50**, 34 (2015).